MOLECULAR SIMULATION
https://doi.org/10.1080/08927022.2021.1873321

Taylor & Francis
Taylor & Francis Group

In silico study of the interactions of *Pilocarpus microphyllus* imidazolic alkaloids with the main protease (M^{pro}) of SARS-CoV-2

Ézio R. A. de Sá[a], Allan N. Costa[b], Rayla K. M. Costa[c], Janilson L. Souza[d], Ricardo M. Ramos[e] and Francisco das C. A. Lima[c]

[a]Federal Institute of Education, Science and Technology of Piauí, IFPI, Picos, Brazil; [b]Federal Institute of Education, Science and Technology of Pará, IFPA, Conceição do Araguaia, Brazil; [c]Research Laboratory of the Computational Quantum Chemistry and Drug Planning Group, Chemistry Department, State Univerty of Piauí, GQQC&PF/UESPI, Teresina, Brazil; [d]Federal Institute of Education, Science and Technology of Maranhão, IFMA, Bacabal, Brazil; [e]Research Laboratory in Information Systems, Information Department, Environment, Health and Food Production, Federal Institute of Education, Science and Technology of Piauí, LaPeSI/IFPI, Teresina, Brazil

ABSTRACT

The disease outbreak caused by SARS-CoV-2 continues to rise worldwide, even in countries which have considered it controlled. As new cases appear daily, infecting millions of people and causing thousands of deaths, the current *in silico* study aims to investigate the imidazolic alkaloids of the species *Pilocarpus microphyllus* (Jaborandi) as a potential inhibitory activity against the M^{pro} protease from SARS-CoV-2, since it plays a fundamental role in the processing of polyproteins that are translated from viral RNA. Jaborandi is distributed in some Brazilian biomes, being easily identified, yet little researched, with proven anti-inflammatory, contraceptive, anti-diabetic and gastroprotective activities. In this work, DFT calculation of thermodynamic properties, electrostatic potential surface, frontier molecular orbitals and descriptors of chemical reactivity of imidazolic alkaloids were associated with the use of molecular docking techniques, molecular dynamics and ADMET predictions. One can verify a good reactivity chemistry and energetic stability of epiisopiloturine, epiisopilosine, isopilosine and e pilosine with some residues of amino acids present in the active site of the main protease of COVID-19. In this sense, the results point out to the imidazolic alkaloids of Jaborandi as promising targets for *in vitro* and *in vivo* tests, as possible candidates for inhibitors of the enzyme M^{pro}.

ARTICLE HISTORY
Received 16 September 2020
Accepted 3 January 2021

KEYWORDS
COVID-19; molecular docking; molecular dynamics; ADMET predictions; SARS-CoV-2 M^{pro}

1. Introduction

The disease known as COVID-19 is of zoonotic origin and has caused the severe acute respiratory syndrome by coronavirus-2 (SARS-CoV-2) in human beings [1]. In December 2019, the disease was diagnosed for the first time in patients from Wuhan, a city with about 11 million inhabitants, in the capital of the province of Hubei, located in the People's Republic of China [2]. Due to the high rates of the new coronavirus transmission among human beings, on March 11, 2020, the World Health Organization (WHO), classified its contagion as a worldwide pandemic [3].

Hence, SARS-CoV-2 is highly contagious, and easily transmitted through respiratory droplets released into the air by infected people through their coughing or sneezing [1]. According to the Pan American Health Organization, PAHO/WHO Brazil (https://www.paho.org/bra/), by November 30 of 2020, there are a total of 62.363.527 cases (496.892 new cases compared to the previous day) and 1.456.687 deaths (7.697 new deaths in relation to the previous day), resulting from COVID-19 [4].

After investigating the coronavirus organism, the researchers found that its main SARS-CoV-2 protease (M^{pro}) is an essential enzyme for processing the polyproteins translated from viral RNA. Thus, by blocking the process in one of the main steps (the cleavage of precursor polyproteins), the vital cycle of viral reproduction would be impaired [5]; indicating it to be a promising target for the development of drugs to combat SARS-CoV-2 [6,7].

The crystallographic structure of M^{pro} complexed to the N3 ligand was recently deposited in the Protein Data Bank (PDB) with a resolution of 2.16 Å [8]. Since N3 is a Michael acceptor inhibitor, developed by a computer aided drug design, it is able to specifically inhibit M pro from multiple coronaviruses, including SARS-CoV and MERS-CoV [9,10]. It is covalently linked to the receptor and is being investigated *in silico* and *in vitro* to discover the mechanism of action against this protease [8].

It is well known that natural herbal medicines are important sources of active ingredients for the treatment of diseases. Affected by the traditional medicine, which effectiveness comes from medicinal plants use, the modern medicine also uses many of these effective healing agents [11]. In this scenario, the researches involving extracts of medicinal plants are very relevant, as there is an enormous biodiversity in Brazil, which enables the large-scale investigation of substances with pharmacological activities not unknown by science [12].

For instance, it is possible to mention the use of the plant species *Pilocarpus microphyllus Stapf ex Wardleworth,* belonging to the *Rutaceae* family, originally from the North and Northeast regions of Brazil, popularly known as Jaborandi,

CONTACT Francisco das C. A. Lima fdcalima@gmail.com

with important medicinal properties; but with applications still little known [13].

The extract of *P. microphyllus* is indicated for the treatment of the flu, fever, inflammation, pneumonia, asthma, glaucoma, diabetes, rheumatism, and others [14]. It also has antidiabetic activities [15], and among its constituents which have already been investigated are: pilocarpine, in the use of glaucoma and xerostomia treatment [16,17]; epiisopiloturine, in the fight against schistosomiasis [18–20]; as well as anti-inflammatory, contraceptive [21] and gastroprotective activities [22]; and the molecules of epiisopilosine and isopilosine with pharmacological action against *S. mansoni* [23]. Under those circumstances, the phytomolecules of Jaborandi become promising targets for the study of the properties not known or little described in the literature.

Given the importance and the urge of the discovery, in conjunction with the planning of new drugs, molecular modelling emerges as a powerful technique, which provides a set of tools to be used in the processes of identification, selection, manipulation, optimisation and characterisation of new drug candidates, due to its high capacity for forecasting and obtaining the thermodynamic, energetic and structural properties of the complexes (receptor–ligand) analysed [24].

Accordingly, the molecular docking method has stood out as an important fitting tool for predicting interactions between macromolecular ligands and receptors [25]. In addition to it, the molecular dynamics has also shown expressive importance through the investigation of variations in the movement of ligands over time, the mechanism of diffusion, the folding of molecular chains and structural changes caused by interactions at receptor binding sites [24]. Regarding the pharmacokinetic properties *in silico*, it has been an investigative approach widely used in the initial study of the properties of Absorption, Distribution, Metabolism, Excretion, and Toxicity (ADMET), reducing costs with biological tests of unattractive substances, and providing greater agility in drug selection [26].

Therefore, as there are still no drugs available and effective treatments for the cure of COVID-19, the present *in silico* study aims to investigate the reactivity and chemical interaction of imidazolic alkaloids of the species *Pilocarpus microphyllus* (Jaborandi) with the M^{pro} protease of SARS-CoV-2.

2. Computational details

2.1. 3d structure of ligands and receptors

The crystal structure of the SARS-CoV-2 M^{pro} receptor (PDB code: 6LU7) was obtained from the Protein Data Bank [8,27]. The three-dimensional structures of the ligands Pilosine (PS), Isopilosine (IPS), Epiisopilosine (EPS), Epiisopiloturine (EPR), Pilocarpine (PC), Isopilocarpine (IPC), Pilocarpidine (PD), Isopilocarpidine (IPD), Pilosinine (PN) e 13-nor-7 (11) -dehydro-pilocarpine (13N), (11) -dehydro-pilocarpine (13N), found in the extract of Jaborandi leaves [23,28–30], were built with the GaussView software version 6 [31].

2.2. Computational calculations

In order to obtain the global minimum energies, thermodynamic properties, Molecular Electrostatic Potential Surface (MEPS), frontier molecular orbitals and descriptors of the global chemical reactivity of the ligands, calculations geometric optimisation and frequency in the gas phase (vacuum system) were performed, at the level of Density Functional Theory (DFT) and based on studies by Rocha et al. [20] and Costa et al. [32,33]. For this purpose, it was used the Gaussian 09 software [34] and the B3LYP hybrid method [35,36] associated with the basis set 6-311++G(d,p) [37,38]. The descriptors of global chemical reactivity were determined based on the theorems of Janak [39], Perdew et al. [40] and Parr et al. [41,42].

2.3. Molecular docking

The preparation of the ligands and the receptor, just as the visualisation of the complexes, were carried out with the UCSF Chimera software [43]. During the protease preparation phase, water molecules and the N3 crystallographic ligand were removed. The addition of hydrogen, the calculation of the Gasteiger loads of the receptor, and ligands were performed using the AutoDock Tools (ADT) software, version 1.5.6 [44,45]. Molecular docking calculations were performed with AutoDock Vina [46] software. During the process, the receptor was considered as a rigid structure and the ligands as flexible ones [47]. The Met165 residue was chosen because it is part of the active M^{pro} protease site and performs interactions with the side chains of the N3 ligand [8], being your cartesian coordinates ($x = -16.406$, $y = 13.719$ and $z = 67.212$) used to define the centre of the grid box [27].

In the Autodock, the Lamarckian genetic algorithm was used as a research parameter [48]. The size of the cubic box generated by AutoDocK Vina, in the region of the receptor interaction, was defined as 22.5 Å for each cartesian axis, the number of modes was set to 50, and the exhaustiveness to 24 [49]. The analysis of molecular docking was concentrated in the lower energy clusters, with the most stable conformation being chosen. The binding energy of the N3 critalographic ligand was calculated by molecular docking as an observation model for the imidazolic alkaloids of Jaborandi. Intermolecular interactions (hydrogen bonds, electrostatic, van der Waals and hydrophobic contacts) were identified and visualised by the Discovery Studio Visualizer 2020 software [50].

2.4. Molecular dynamics

The initial coordinates for the molecular dynamics simulations were obtained from the complexes with the lowest binding energy, determined by molecular docking. The CHELPG method (CHarges from ELectrostatic Potentials using a Grid-based method) was applied to obtain the atomic charges of the ligands [51], based on the data presented in the literature [52,53], and from the geometric optimisation calculations with the B3LYP/6-311++G(d,p) model and use the Gaussian 09 software [34].

For the protonation of the SARS-CoV-2 M^{pro} enzyme, the H++ online server was used [54]. The molecular dynamics simulations were performed with the GROMOS96 force field 53a6 included in the GROMACS package, version 2018.1 [55,56]. The systems were simulated using the NPT set (in which the number of particles, pressure, and temperature are

constant), and periodic boundary conditions (cubic) [57]. The water molecules during the process were made explicit by the Single Point Charge (SPC) model [58]. The simulation time was 50 nanoseconds (ns), with an integration step of 2 fs [59]. The systems were gradually warmed up, starting with 100 K (10 ps), 150 K (5 ps), 200 K (5 ps), 250 K (5 ps), and later being adjusted to 310 K [57]. The initial 6 ns of each simulation were considered as part of the heating (0.025 ns) and equilibrium (5.975 ns) steps, not being used in the data analysis [57].

The temperatures of solvent and solutes (protein, ligands, water, and sodium ions) were independently coupled to a thermal bath with a relaxation time of 0.1 ps using the V-rescale thermostat [57]. The pressure in the system was weakly coupled to a pressure bath with 2 ps of relaxation time, using the Parrinello-Rahman barostat [60,61]. Bond lengths were constrained using the LINCS algorithm [62], and electrostatic interactions among non-ligand atoms were evaluated by the Particle Mesh Ewald (PME) method [63]. GROMACS provides the ability to calculate the energies of short-range (Lennard-Jones potential) and long-range (Coulomb potential) unbound interactions and their error estimates for the receptor–ligand complexes [64,65], being the sum of the energies realised posteriorly. The visualisation and graphic production of the results happened throughout the use of the UCSF Chimera software [43].

2.5. ADMET predictions

The obtaining of the physicochemical and pharmacokinetic properties of the ligands occurred through the *in silico* search, using the structures (2D, 3D or SMILES) on the online platforms: PreADMET [66], FAF-Drugs4 [67], SwissADME [68] and PASS Oline [69].

Some of the parameters analysed were: Human Intestinal Absorption (HIA), Penetration in the Blood–brain Barrier (BBB), Lipinski's rule, permeability in Caco2 and MDCK cells (Madin-Darby canine kidney), aqueous solubility, the mutagenicity of species Ames Salmonella (TA100 and TA1535), the carcinogenicity, mutagenicity and bioactivity assays [70].

3. Results and discussion

3.1. Energetic properties of the ligands

The 3D structures of the molecules (Figure 1): pilosine, isopilosine, epiisopilosine, epiisopiloturine, pilocarpine, isopilocarpine, pilocarpidine, isopilocarpidine, pilosinine and 13-nor-7 (11)-dehydro-pilocarpine, are the most stable for the model B3LYP/6-311++ G(d,p).

In this study, it is possible to detect the existence of four isomeric forms ($C_{16}H_{18}N_2O_3$) for the alkaloids EPR (Figure 1a), EPS (Figure 1b), IPS (Figure 1c) and PS (Figure 1d). The presence of optical isomerism in the EPS, IPS and PS molecules is perceived, according to the results of Rocha et al. [20], observed through the rotation of two conforming atoms (C4 and C9), and by the presence of three chiral carbons (C5, C7, and C8), which corroborate with the data presented in the experimental studies of Rocha et al. [23].

It also points out Rocha et al. [20] that the chemical structure of these alkaloid isomers has a difference in stability between their dihedral angles. Because, when acquiring a cis-like geometric conformation, the PS alkaloid (Figure 1d) tends to be less stable than the EPR (Figure 1a), demonstrating to be the most stable one due to its trans-type geometric configuration. Then, the frequency calculations were performed to determine the thermodynamic properties of imidazolic alkaloids, as shown in Table 1.

It can be seen in Table 1, the proposed model describes the energetic properties of the systems well, demonstrating that these data correspond to the thermodynamically more stable structures for the respective ligands (Figure 1). However, those with the lowest energy values of the parameters: zero-point, thermal energy, enthalpy, and Gibbs free energy, are considered the most stable ones. Thus, the best results are found in the compounds EPR, EPS, IPS, and PS respectively, indicating a great similarity between their energy parameters, possibly caused by the phenomenon of isomerism. Meanwhile this, the least stable is the PN molecule, due to its associated value, caused by the different geometric properties.

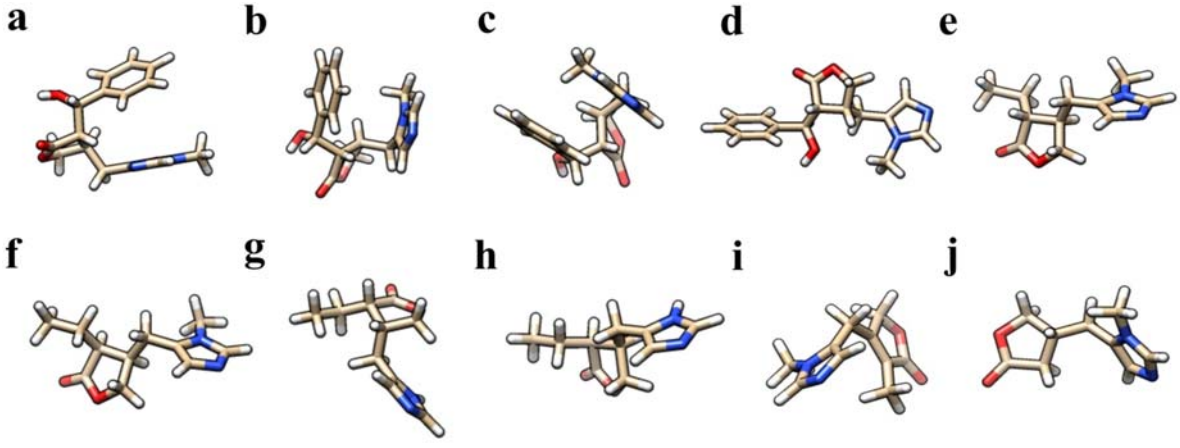

Figure 1. The most stable 3D structures for **(a)** EPR, **(b)** EPS, **(c)** IPS, **(d)** PS, **(e)** PC, **(f)** IPC, **(g)** IPD, **(h)** PD, **(i)** 13N and **(j)** PN were obtained from geometric optimisation calculations using the B3LYP/6-311++G(d,p) model. Atoms are represented by the colours: Carbon (beige), Hydrogen (white), Nitrogen (blue) and Oxygen (red).

Table 1. Increasing order of the energetic values of the imidazolic alkaloids of the species *P. microphylus* determined by the model B3LYP/6-311++ G(d,p).

	Energy (kcal mol^{-1})			
Alkaloides	HF[a]	ΔT[b]	ΔH[c]	ΔG[d]
EPR	-5.99688×10^5	-5.99676×10^5	-5.99675×10^5	-5.99719×10^5
EPS	-5.99686×10^5	-5.99674×10^5	-5.99674×10^5	-5.99717×10^5
IPS	-5.99686×10^5	-5.99674×10^5	-5.99674×10^5	-5.99717×10^5
PS	-5.99685×10^5	-5.99673×10^5	-5.99672×10^5	-5.99716×10^5
PC	-4.32163×10^5	-4.32154×10^5	-4.32153×10^5	-4.32190×10^5
IPC	-4.32160×10^5	-4.32151×10^5	-4.32150×10^5	-4.32188×10^5
IPD	-4.07506×10^5	-4.07498×10^5	-4.07498×10^5	-4.07532×10^5
PD	-4.07505×10^5	-4.07497×10^5	-4.07497×10^5	-4.07531×10^5
13N	-4.06755×10^5	-4.06746×10^5	-4.06746×10^5	-4.06781×10^5
PN	-3.82845×10^5	-3.82837×10^5	-3.82837×10^5	-3.82870×10^5

[a]Zero energy point; [b]Thermal energy; [c]Enthalpy; [d]Free energy Gibbs.

However, it is necessary to understand that properties, such as enthalpy and entropy, can undergo energetic changes, according to the contributions caused by the vibrational, translational, rotational, and electronic movements of the molecules [71].

3.2. Electrostatic potential maps

MEPS is a map that represents the distribution of electronic density on the surface of a molecule. This one is widely applied in predicting sites and relative reactivity for electrophilic attack, in studies of biological recognition and interactions by hydrogen bonds. Figure 2 shows the imidazolic alkaloids, in which the negative electrostatic potential (in red) represents the attraction of the proton by the region of high concentration of electrons in the molecule, whereas the positive electrostatic potential (in blue) corresponds to the repulsion of the proton by atomic nuclei [32].

It is possible to observe, in Figure 2, the electronic density for each molecule is represented by red regions (polar and negatively charged) and blue regions (non-polar and positively charged). A greater electron density is present around the nitrogen atom (N3) of the imidazolic ring and the oxygen atoms (O1 and O3) of the γ-butyrolactone ring (oxolan-2-one), thus representing the most likely locations for the occurrence of chemical interactions.

3.3. Chemical reactivity descriptors

The energy of the frontier molecular orbitals, HOMO (Highest Occupied Molecular Orbital) and LUMO (Lowest Unoccupied Molecular Orbital), provides information about the donor and acceptor electron character, respectively, of a compound [72]. The HOMO and LUMO are mainly responsible for the biological interactions between ligands and proteins in a complex [73–75].

The energy values of the HOMO and LUMO orbitals are fundamental to determine the electrical properties, kinetic stability, and the descriptors of global chemical reactivity in a molecule [33]. Thus, Table 2 contains some electronic properties determined from the calculation method B3LYP/6-311++ G(d,p) used for the imidazolic alkaloids of the species *P. microphyllus*.

It is observed that the compounds, in Table 2, demonstrate a similarity in the electronic properties, however, the substance EPR stands out in relation to its greater capacity for charge

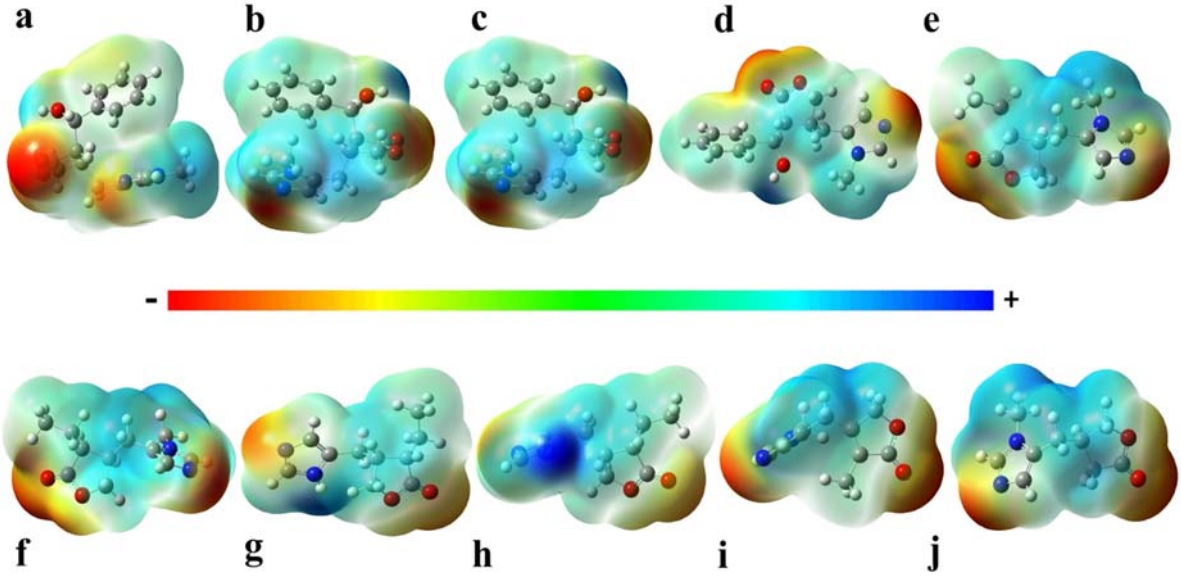

Figure 2. MEPS for **(a)** EPR, **(b)** EPS, **(c)** IPS, **(d)** PS, **(e)** PC, **(f)** IPC, **(g)** IPD, **(h)** PD, **(i)** 13N and **(j)** PN, calculated using the model B3LYP/6-311++ G(d,p). Atoms are represented by the colours: Carbon (grey), Hydrogen (white), Nitrogen (blue) and Oxygen (red).

Table 2. Approximated values of the frontier molecular orbitals and the global reactivity descriptors of the imidazolic alkaloids of the species *P. microphyllus* determined by the method B3LYP/6-311++G(d,p).

	Energy (eV)						
Alkaloides	HOMO	LUMO	μ[a]	χ[b]	η[c]	S[d]	ω[e]
EPR	−6.45	−0.70	−3.57	3.57	2.88	0.35	2.22
EPS	−6.40	−0.96	−3.68	3.68	2.72	0.37	2.49
IPS	−6.40	−0.96	−3.68	3.68	2.72	0.37	2.49
PS	−6.33	−0.96	−3.64	3.64	2.68	0.37	2.47
PC	−6.51	−0.74	−3.62	3.62	2.88	0.35	2.27
IPC	−6.50	−0.80	−3.65	3.65	2.85	0.35	2.33
IPD	−6.55	−0.65	−3.60	3.60	2.95	0.34	2.20
PD	−6.64	−0.87	−3.75	3.75	2.88	0.35	2.44
13N	−6.61	−1.50	−4.05	4.05	2.56	0.39	3.21
PN	−6.52	−0.81	−3.66	3.66	2.85	0.35	2.35

[a]Chemical potential; [b] Electronegativity; [c] Hardness; [d] Softness; [e] Electrophilicity index.

transfer based on its chemical potential (−3.57 eV). The EPS, IPS and PS molecules have a better donor electron character (nucleophilic), and acceptor electron character (electrophilic) in relation to the others molecules. With based in the HOMO and LUMO energies, this molecules show a good chemical reactivity. The 13N molecule has the lowest LUMO energy (−1.50 eV) and thus the least resistance to electron acceptance due to its high electronegativity (4.05 eV), low hardness (2.56 eV), high smoothness (0.39 eV) and the best index of electrophilicity (3.21 eV).

Concerning the chemical hardness, a large difference in energy gap between HOMO and LUMO characterises a molecule as being hard and is related to more stable molecules, while a small difference in energy gap corresponds to a molecule as being soft and it is related to more reactive molecules [33].

It can be seen, in Figure 3, the energy gap values for the imidazolic alkaloids are very close; however, the molecules of 13N (5.11 eV), PS (5.37 eV), EPS (5.44 eV) and IPS (5.44 eV) have the smallest chemical gaps and hardness in relation to the others molecules and it can be considered the most reactive.

3.4. Molecular docking

After obtaining the electronic and energetic properties of the imidazolic alkaloids present in the extract of the leaves of Jaborandi, the molecular docking was performed with the

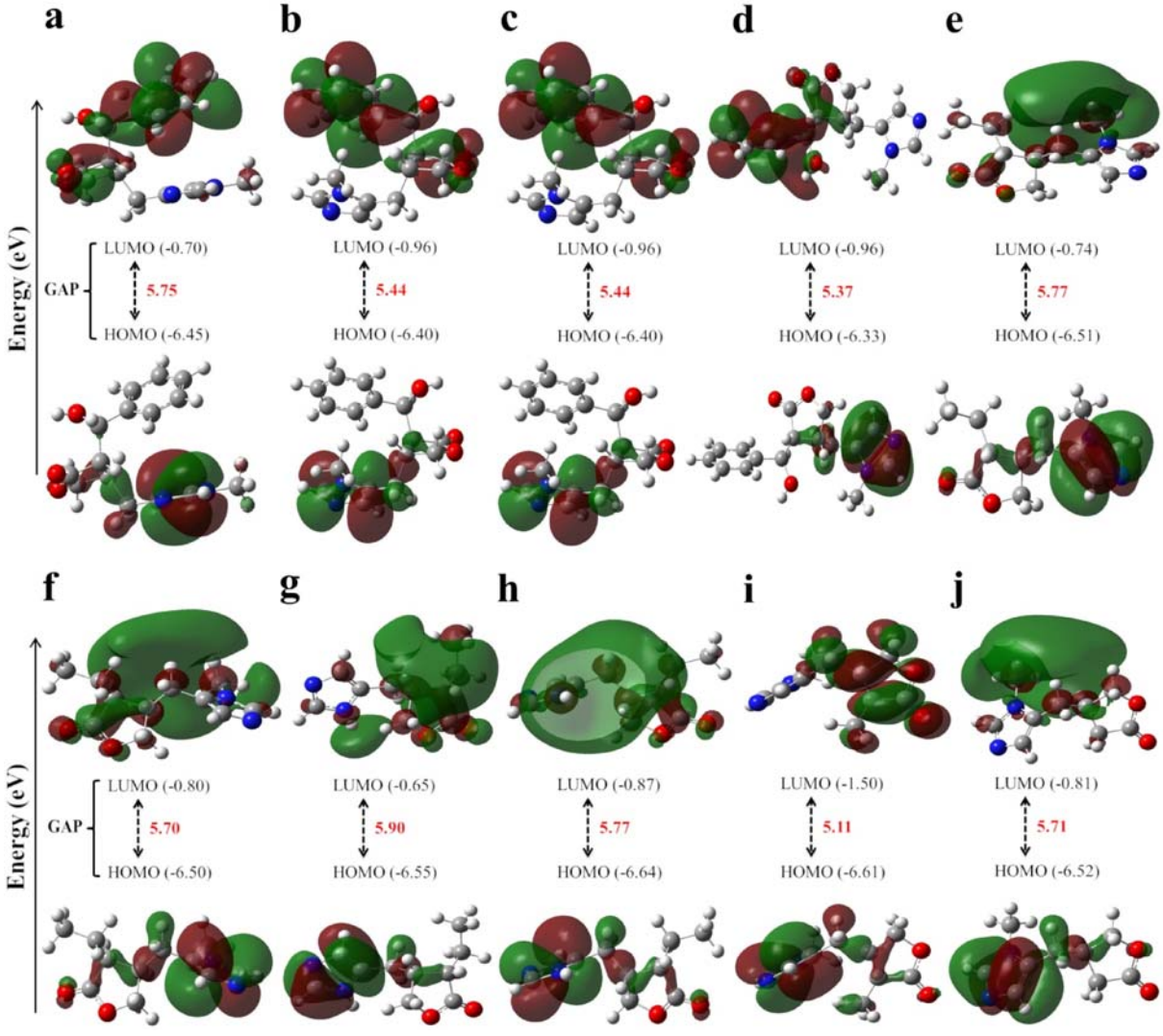

Figure 3. Frontier molecular orbitals and energy gaps for **(a)** EPR, **(b)** EPS, **(c)** IPS, **(d)** PS, **(e)** PC, **(f)** IPC, **(g)** IPD, **(h)** PD, **(i)** 13N and **(j)** PN, calculated using the model B3LYP/6-311++ G (d, p). Atoms are represented by the colours: Carbon (grey), Hydrogen (white), Nitrogen (blue) and Oxygen (red).

Table 3. Values of the binding energies of the imidazolic alkaloids of the species *P. microphyllus* and the N3 ligand with the M^{pro} protease from SARS-CoV-2 determined by molecular docking.

Ligand	N3[a]	EPR	EPS	IPS	PS	IPC	13N	PD	PN	IPD	PC
ΔG^{b}_{bind} (kcal mol^{-1})	−8.3	−7.0	−6.8	−6.8	−6.7	−5.4	−5.3	−5.3	−5.3	−5.1	−5.0

[a]Critalographic ligand (reference); [b] Binding energy (AutoDock Vina).

SARS-CoV-2 M^{pro} protease, responsible for the severe acute respiratory syndrome in humans. Table 3 shows the results of the binding energies found for the imidazolic alkaloids and the N3 critalographic ligand.

As a matter of demonstrating the activity with the active site of the protease M^{pro}, Table 3 shows the ligands EPR (ΔGbind = −7.0 kcal mol^{-1}) and EPS (ΔGbind = −6.8 kcal mol^{-1}) have the best interaction energies with the peptidase. Therefore, EPR was the alkaloid that came closest to the binding energy carried out by the crystallographic ligand N3 (ΔGbind = −8.3 kcal mol^{-1}), accompanied by the isomers EPS, IPS (ΔGbind = −6.8 kcal mol^{-1}) and PS (ΔGbind = −6.7 kcal mol^{-1}). Meanwhile, the PC has the highest interaction energy value (ΔGbind = −5.0 kcal mol^{-1}). Because they are isomeric compounds, the results of the binding energies for these molecules are very close, with similar interactions at the active site of the receptor (Table 4).

In the *in silico* study carried out by Huynh et al. [1], the interactions of the molecules (chloroquine, bromhexine, favipiravir, dipyridamole, ambroxol, hydroxychloroquine, montelukast, cinaserin, GS-441524, kaempferol, lopinavir, entecavir, umifenovir, quercetin, remdesivir, nelfinavir, curcumin, and N3), were analysed along with the SARS-CoV-2 protease M^{pro} through molecular docking with the AutoDock Vina software. In which, N3 was considered as the control molecule, which showed an important interaction at the binding site with one of the best fitting scores, estimated at −7.1 kcal mol^{-1}. In this sense, the relevance of the binding energies presented by the imidazolic constituents of the Jaborandi leaf is perceived, mainly the molecules that are isomers to EPR.

It is possible to establish a relationship between a molecular docking study carried out by Barros et al. [49], which was relevant when investigating the interaction activity of 24 ligands (based on commercialised drugs), and four SARS-CoV-2 receptors, presenting a M^{pro} with a stable ΔGbind when coupled with the drugs Pemirolast (−5.8 kcal mol^{-1}), Benserazide (−4.9 kcal mol^{-1}) and Luteolin (−6.1 kcal mol^{-1}). The results presented are as important as those of the aforementioned study, since the energy of interaction of the imidazolic alkaloids EPR, EPS, IPS and PS of Jaborandi with M^{pro} (Table 3) were very favourable to the receptor–ligand interaction.

Table 4 shows the best molecular affinity results, for imidazolic alkaloids and their respective intermolecular interactions (hydrogen, electrostatic, hydrophobic, and van der Waals bonds), with some amino acid residues in the active site of the main peptidase of COVID-19.

By drawing a parallel based on the crystallographic results of the SARS-CoV-2 protease M^{pro}, each protomer is formed by the junction of three domains: Domain I (residues 8–101), Domain II (residues 102–184) and domain III (residues 201–303). The peptidase presents a catalytic dyad composed by the amino acid residues: Cysteine and Histidine; and the substrate binding site represented by a cavity between domains I and II [8]. In brief, it is noticed that the ligands in Table 4 are located in the same region and present similar interactions with the main residues of the active protease M^{pro} site.

The EPS and IPS ligands (Table 4 and Figure 4) when interacting with the protease, present hydrogen bonds with the His41 and Gln189 residues, and electrostatic interactions with His41 and His163; the hydrophobic contacts with His41, Cys145, and His163; however, they differ regarding the van der Waals bonds with the amino acids Leu141 and Ser144, respectively.

While in Figure 5, the PS shows a similarity in relation to the hydrogen bonding to Gln189, the electrostatic interactions with His41 and His163, the hydrophobic contacts with His41 and Cys145, and the van der Waals bonds (His164, Gly143, Asn142, Phe140, His172, Glu166, Tyr54, Arg188, and Asp187). EPR makes contacts with other residues, differentiating in hydrogen bonds when interacting with Thr190 and Gln192, having no electrostatic interactions, presenting hydrophobic contacts with Met49, Met165, and Gln189, and van der Waals connections with Ala191, Leu167, Glu166, and Asp187.

Table 4. Molecular affinity parameters of imidazolic alkaloids of the species *P. microphyllus* with lower binding energies with the active site of the protease M^{pro} of SARS-CoV-2.

	Amino acids residues with interactions[a]			
Ligand	Hydrogen Bonds	Electrostatic	Hydrophobic	van der Waals
EPR	Thr190, Gln192	–	Met49, Met165, Gln189	Ala191, Leu167, Glu166, Asp187
EPS	His41, Gln189	His41, His163	His41, Cys145, Leu141, His163	His164, Gly143, Asn142, Phe140, His172, Glu166, Met165, Tyr54, Arg188, Asp187, Leu27, Leu 141
IPS	His41, Gln189	His41, His163	His41, Cys145, His163	His164, Gly143, Asn142, Phe140, His172, Glu166, Met165, Tyr54, Arg188, Asp187, Leu27, Ser 144
PS	Cys145, Gln189	His41, His163	His163, Cys145, Met49, Met165	His164, Gly143, Asn142, Phe140, His172, Glu166, Tyr54, Arg188, Asp187, Ser 144

[a]Obtained using Discovery Studio Visualizer 2020.

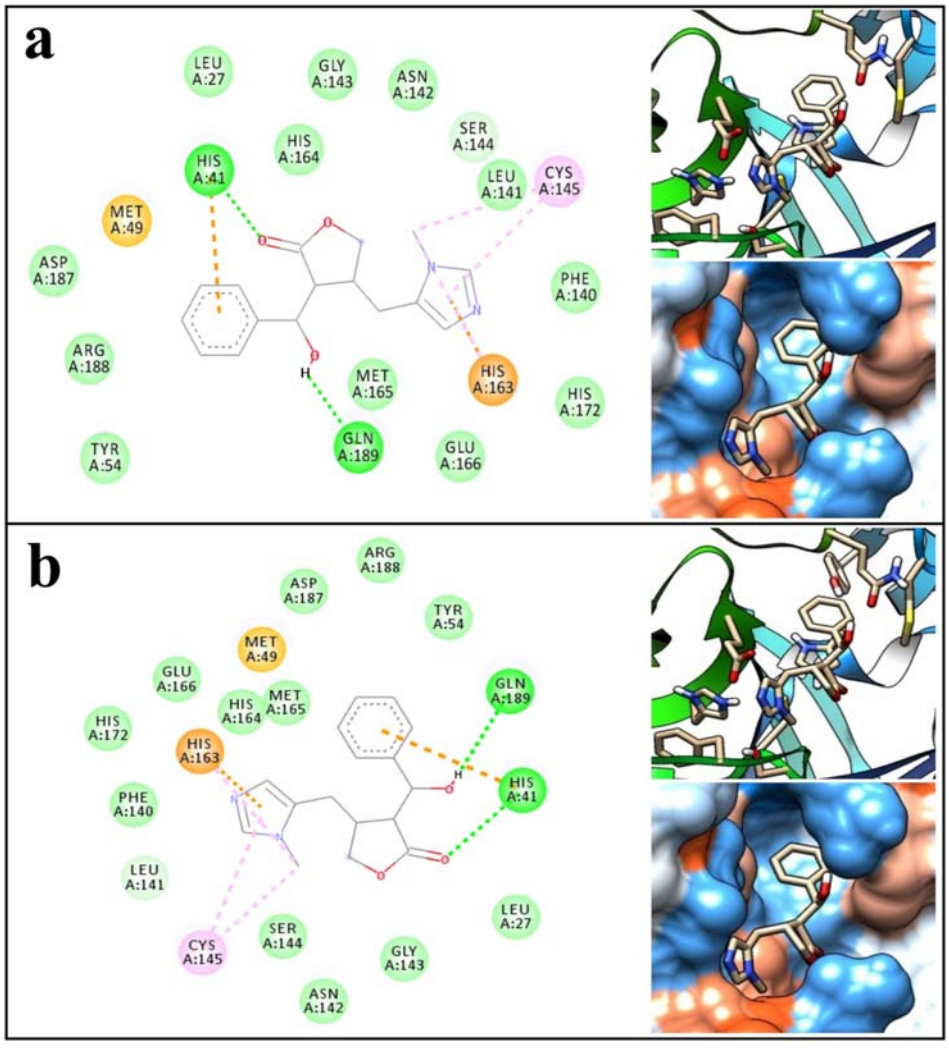

Figure 4. Intermolecular interactions between residues of the active site of the protease M^{pro} and the molecules **(a)** EPS and **(b)** IPS in 2D and 3D. Residues and bonds are represented by colours: Hydrogen bonds (green), Electrostatics (orange), Hydrophobic contacts (pink) and van der Waals (light green). Hydrophobic region of the active site (red surface) and hydrophilic protein region (blue surface).

Figure 4 (**a** and **b**) shows all interactions carried out after molecular docking with EPS (Figure 4a) and IPS molecules (Figure 4b), in which is visible the hydrogen bond between oxygen (O3) of the ester organic function of the γ-butyrolactone ring (oxolan-2-one) with the His41 residue, and a second hydrogen bond (H29) of the hydroxyl group of the alcohol organic function with the amino acid Gln189.

In Figure 5 (**a** and **b**), all interactions performed after molecular docking are illustrated. It is noticed in the EPR (Figure 5a), the existence of a hydrogen bond between the oxygen (O3) of the organic ester function of the γ-butyrolactone ring with the Gln192 residue, and a second bond occurs between the hydrogen (H29) of the hydroxyl group of the alcohol organic function with the amino acid Thr190. While in PS (Figure 5b), a hydrogen bond is created between the oxygen (O1) of the organic ester function of the γ-butyrolactone ring with the Cys145 residue, and a second bond between the hydrogen (H29) of the hydroxyl group of the alcohol organic function with the amino acid Gln189. This fact is observed in the crystallographic structure of the protease M pro, in which, through electronic density, the crystallographic ligand N3 performs a 1.8 Å covalent bond with the Cys145 of the binding site [8].

It is noticed that the EPR and EPS molecules have the best interaction affinities, based on the binding energies with the enzyme M^{pro} (Table 3). This can be justified by the location, the type of connection, and the position of the ligands in the active site. According to Huynh et al. [1], after studies of docking and molecular dynamics with 19 drug molecules, it was observed that the 'anchor' site at the protease binding site M^{pro}, plays an important role in the stabilisation of ligands, caused by hydrophobic interactions performed. In the crystallographic structure of the M^{pro} peptidase from SARS-CoV-2 complexed to N3, one end of the ligand occupies the 'anchor' site of the active site, which was revealed as an important region for the interaction with the receptor [1].

Agents capable of inhibiting the SARS-CoV-2 protease M^{pro} are essential to blocking viral replication [5]. In this binding site, there are the amino acid residues His41, Met49, Gly143, Cys145, His163, His164, Glu166, Pro168, and Gln189, as shown in the recent study on α-ketoamide inhibitors [5]. In the present study, it was possible to identify the

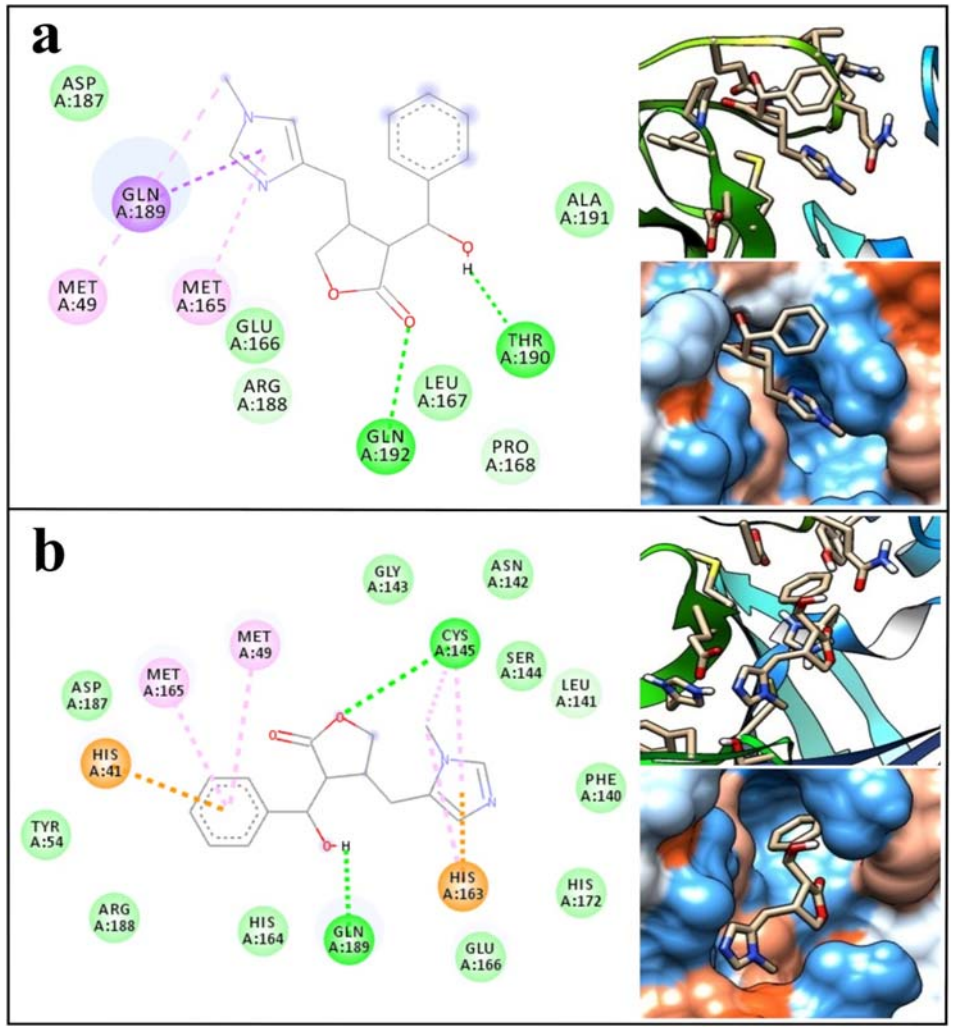

Figure 5. Intermolecular interactions between the residues of the active site of the protease M^{pro} and the molecules **(a)** EPR and **(b)** PS in 2D and 3D. Residues and bonds are represented by colours: Hydrogen bonds (green), Electrostatics (orange), Hydrophobic contacts (pink / purple) and van der Waals (light green). Hydrophobic region of the active site (red surface) and hydrophilic protein region (blue surface).

presence of the same amino acid residues by performing different interactions with the ligands EPR, EPS, IPS, and PS, thus being considered as strong candidates for the enzymatic inhibition of M^{pro} in COVID-19.

3.5. Molecular dynamics

Molecular dynamics calculations were performed based on the most stable conformations of the ligands determined by molecular docking. The M^{pro}-EPR and M^{pro}-EPS complexes were selected for the 50 ns simulations, using the amino acid residue Met165 as a reference located at the active site of the protease. Thus, it can be seen, in Figure 6, that the EPR ligand has a good interaction with the site, very close to the selected residue, in the intervals of 6–20 ns, 24–27 ns, 29–35, 42 ns and 44–50 ns, and remaining out of that location in two short time intervals 21–23, 28 ns, 36–41 and 43 ns. Throughout this simulation, a constant change in the conformation of the M^{pro}-EPR complex is noticeable. All things considered, the results reproduce the system well, presenting a good connection affinity in most of the simulation.

It is observed, in Figure 7, the behaviour of the binding affinity in the M^{pro}-EPS complex during the simulation time, in which the ligand in the period from 6 to 50 ns shows a good interaction, remaining in the binding site. The occurrence of a high thermodynamic stability is shown, due to the energetic balance between the ligand and the active site of the protease, then providing the stabilisation of the complex attributable to the interactions carried out with the residues of that region.

The M^{pro}-EPS complex, in Figure 7, presents different conformations as the simulation time increases, with that, the ligand adjusts geometrically to the active site of the protease as it undergoes structural changes. Figure 8 shows the interaction times in nanoseconds of the M^{pro}-EPS and M^{pro}-EPR complexes during the simulation.

Based on the analysed data, the EPR and EPS molecules when interacting with the SARS-CoV-2 protease M^{pro} have a dynamic and reversible character, caused by the flexibility and structural reorganisation capacity of the complexes during the simulation. Then, when the ligands interact with the peptidase M^{pro}, they assume a new structural conformation. However, when this equilibrium condition is affected,

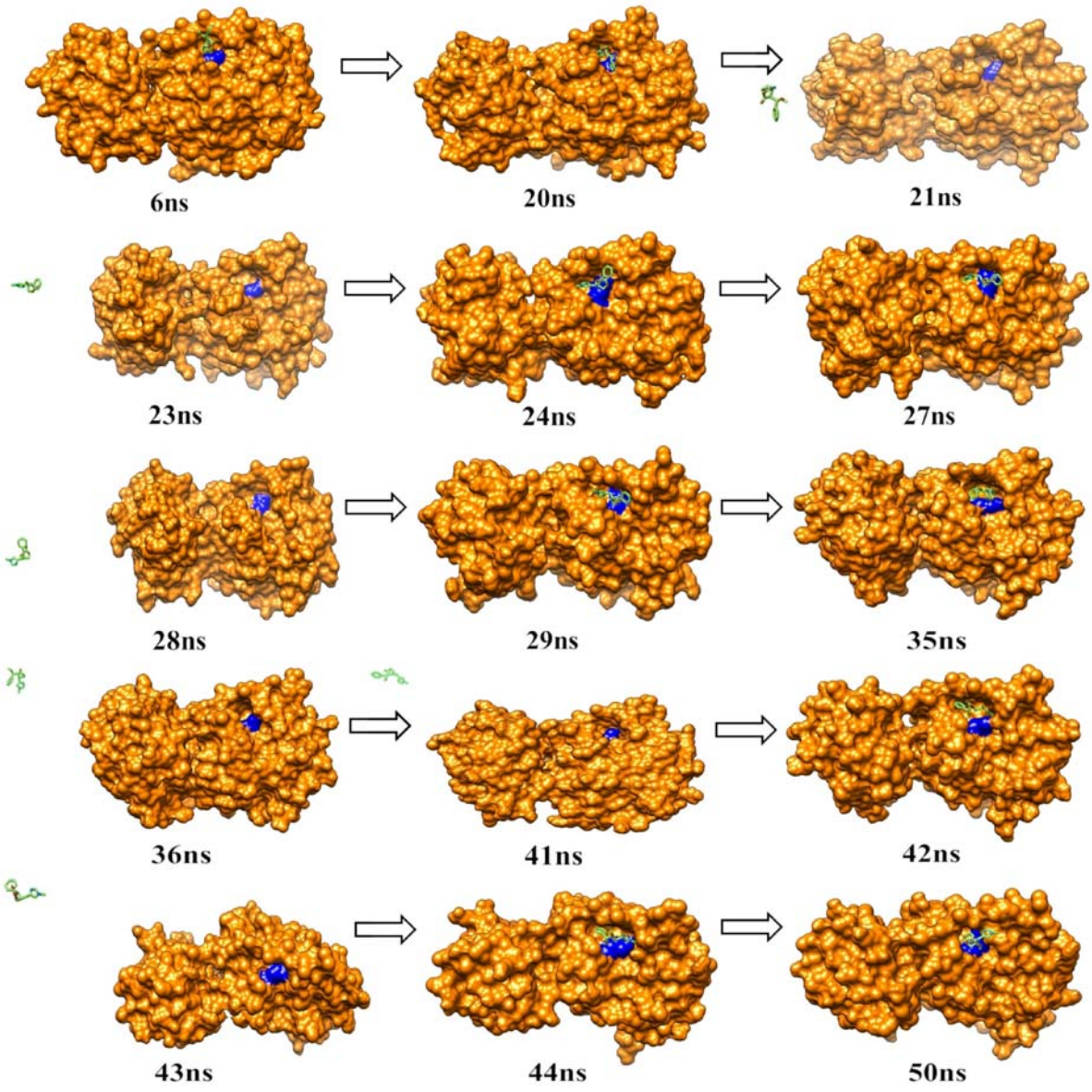

Figure 6. Interaction activity of the M^{pro}-EPR complex simulated by molecular dynamics during the 50 ns time. The colours are only illustrative for the representation of the receptor-ligand complex: protease M^{pro} (orange surface), location of the Met165 residue at the binding site (blue surface) and the location of the EPR ligand (green surface).

it causes a destabilisation of the system and subsequent expulsion of the ligand, as occurred with the EPR. When establishing a new balance, the energy of the system returns to its favourable condition of interaction with the ligand; allowing to return it to the region of the active site of the protease [76].

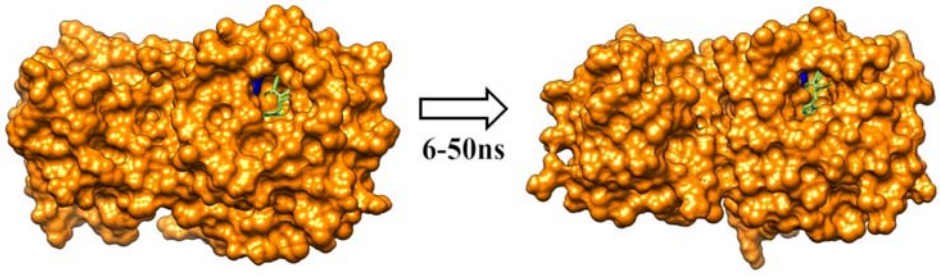

Figure 7. Interaction activity of the M^{pro}-EPS complex simulated by molecular dynamics during the 50 ns time. The colours are only illustrative for the representation of the receptor-ligand complex: protease M pro (orange surface), location of the Met165 residue at the binding site (blue surface) and the location of the EPR ligand (green surface).

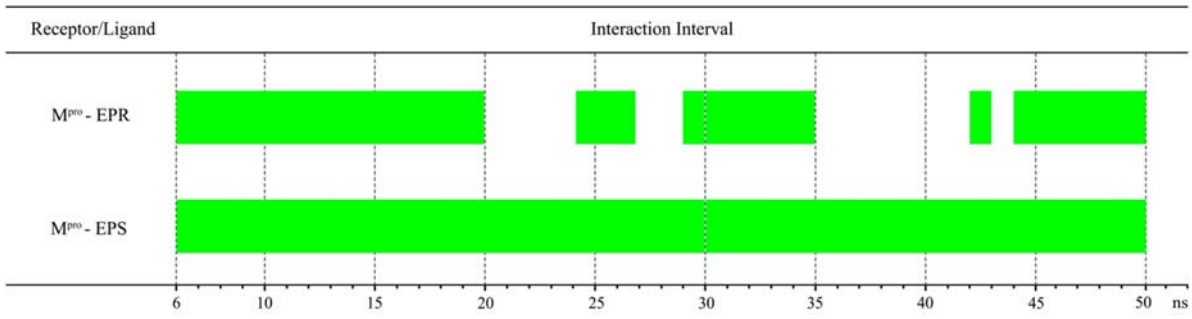

Figure 8. Interval of interaction between ligands and protease M^{pro} during 50 ns of molecular dynamics simulation.

Table 5 shows the values of the energies of electrostatic interactions (Coulomb), by van der Waals (Lennard-Jones) and the sum of these (Coul + LJ), calculated for the M^{pro} complexes of SARS-CoV-2 with the ligands EPS and EPR, during the time of analysis of the simulation by molecular dynamics.

These results in Table 5 show that the EPS ligand features a better Coul energetic interaction (-50.4488 ± 4.9 kJ mol^{-1}) in relation to EPR (-15.5741 ± 4.4 kJ mol^{-1}) when interacting with the enzyme M^{pro}, and this fact is caused by the electrostatic character of the hydrogen bonds formed in the complex. The LJ interactions are present in the two complexes, in which the EPS ligand has the lowest energy (-143.973 ± 2.9 kJ mol^{-1}) compared to the EPR (-122.483 ± 6.0 kJ mol^{-1}). Therefore, we can observe the same behaviour with the approximate sum of the binding energies (Coul + LJ), as the EPS (-194.422 ± 5.7 kJ mol-1) presents greater thermodynamic stability in relation to EPR (-138.057 ± 7.4 kJ mol^{-1}), when the M^{pro} protease of SARS-CoV-2 is complexed. This behaviour can be explained by the longer interaction time and better conformational balance with the binding site. Although EPS is thermodynamically more stable, EPR showed considerable interactions with peptidase M^{pro}. However, the results for the energies in the interaction process between the ligand and the active site of the receptor are not the only determining factor for binding affinity.

3.6. ADMET predictions

The ADMET results of the physical–chemical and pharmacokinetic properties of the EPR, EPS, IPS, and PS molecules are shown in Tables 6–8. It is important to highlight that the EPR, EPS, IPS, and PS isomers have similar or even equal parameters as seen in this section.

The ideal molar solubility in water (logS) should be greater than −4 and less than 6, based on a qualitative solubility estimate provided by the logS scale [68]. Whereas the distribution constant (logD) is a descriptor of lipophilicity, adjusted to a pH using a tampon, its ideal value tends to be greater than 3 [68,77]. In effect, it can be seen in Table 6 that the compounds have low lipophilicity and reasonable hydrophilicity. According to Storpirtis et al. [78], a soluble molecule facilitates many activities for the development of drugs, especially in relation to handling and formulation. On the other hand, when it is insoluble it can hinder the dissolution process in biological fluids and the development of some pharmaceutical forms.

TPSA (Topological Polar Surface Area) is a descriptor commonly related to hydrogen bonds, which can cause changes in permeability and oral bioavailability. It can be used in combination with counting rotatable bonds and assessing molecular flexibility, which can also alter the oral bioavailability of many molecules [79]. The polarity or polar topological surface area must be between 20 and 130 Å2; thereby, the values in Table 6 are in accordance with the ideal value [80].

The Hydrogen Bonding Donor (HBD) and Hydrogen Bonding Acceptor (HBA) are two important factors. Studies show that compounds with a presence of HBA, greater than HBD, are favourable for ADMET conditions, considering that a large number of HBD may result in low permeability, absorption, and bioavailability [81]. Thus, it is observed that the analysed isomers obey the rule (HBD ≤5 and HBA ≤10).

Many rules have been developed to guide the selection of drug candidate compounds [82]. The similarity of drugs was established from structural or physical–chemical inspections of the compounds, the advanced and sufficient development to be considered candidates for oral drugs, according to the parameters established in the filters.

Lipinski's rule, also known as the rule of five, outlined the relationship between pharmacokinetics and physical–chemical

Table 5. Energy values of the average Coulomb (Coul), Lennard-Jones (LJ) interactions, and the approximate sum (Coul + LJ) for the complexes.

Receptor-Ligand	Coul (kJ mol^{-1})	LJ (kJ mol^{-1})	Coul + LJ (kJ mol^{-1})
M ^{pro}- EPR	-15.5741 ± 4.4	-122.483 ± 6.0	-138.057 ± 7.4
M ^{pro}- EPS	-50.4488 ± 4.9	-143.973 ± 2.9	-194.422 ± 5.7

Table 6. Physico-chemical and pharmacokinetic parameters evaluated by the FAFDrugs4 and Swiss ADME software.

Parameter (ideal)	EPR	EPS	IPS	PS
MW[a] (<450)	286.33	286.33	286.33	286.33
logP[b] (≤4.5)	1.59	0.62	0.62	0.62
logD (>3)	1.08	0.96	0.96	0.96
logS[c] (>−4)	−2.56	−1.95	−1.95	−1.95
TPSA[d] (<180)	64.35	64.35	64.35	64.35
HBD[e] (≤5)	1	1	1	1
HBA[f] (≤10)	5	5	5	5
Lipinski Violation (<2)	0	0	0	0
Fsp3[g] (>0.36)	0.38	0.38	0.38	0.38
Bioavailability score	0.55	0.55	0.55	0.55
Result	Accepted	Accepted	Accepted	Accepted

[a]Molecular weight; [b] Octanol-water partition coefficient; [c] Aqueous solubility; [d] Topological polar surface area (Å2); [e] Number of H donor atoms; [f] Number of H receptor atoms; [g] Number of C sp3.

Table 7. ADME-Tox parameters evaluated by the PreADMET software.

Parameter	EPR	EPS	IPS	PS
Drug-likeness				
Rule_of_Five	Suitable	Suitable	Suitable	Suitable
WDI like rule	In 90% cutoff	In 90% cutoff	In 90% cutoff	In 90% cutoff
ADME				
BBB[a]	0.01167	0.01680	0.01680	0.01680
Caco2[b]	21.83930	22.86810	22.86810	22.86810
MDCK[c]	16.04980	9.63097	9.63097	9.63097
HIA[d]	96.05012	96.05012	96.05012	96.05012
Toxicity				
Ames teste[e]	mutagen	mutagen	mutagen	mutagen
TA100 10RLI	negative	negative	negative	negative
TA100 NA	negative	negative	negative	negative
TA1535 10RLI	negative	negative	negative	negative
TA1535 NA	negative	negative	negative	negative
Carcino Mouse[f]	negative	negative	negative	negative
Carcino Rat[f]	negative	negative	negative	negative
Risco hER inib[g]	médium risk	médium risk	médium risk	médium risk

[a]Blood-brain barrier; [b] Permeability test on Caco2 cells; [c] Permeability test on MDCK cells; [d] Human intestinal absorption; [e] Mutagenicity assay; [f] Carcinogenicity assay; [g] Safety test (hERG K channel).

parameters [81], with the following parameters (HBA≤ 10 and HBD≤5; PW≤500 and MlogP ≤4.5). Thus, the four compounds obey all established conditions, not violating this rule.

The parameter Fsp3 defines the molecular complexity, the number of sp3 carbons hybridised in the total count [68]. All compounds have a higher value than recommended, which can imply high aqueous solubility.

The compounds also have a bioavailability score in which the closer to 1, the higher the quality of the molecule as a potential drug candidate [83]. For this reason, the data are favourable to the analysed compounds. Table 7 reproduces the parameters ADME and Toxicity of imidazolic alkaloids.

In Table 7, the Rule of Five and the WDI like rule (PW≤550; HBA≤ 9 and HBD≤5; logP≤5) indicate these molecules as suitable. The last is based on compounds with molecular properties with a limit equal to or greater than 90% of those found in the World Drug Index (WDI), then, the molecules are in accordance with the rule, as they have a 90% cut [84].

The BBB indicates whether the compound is able to overcome the barrier between blood and cerebrospinal fluid [85]. Then, the present molecules have a very low penetration capacity. Caco-2 cells exhibit many of the morphological and functional properties of human intestinal cells, whereas MDCK cells can be used as a good tool for rapid permeability screening [86]. In ADME terms, the results show Caco-2 with average values and MDCK with small values.

Table 8. Profile of biological activities assessed by PASS Online.

Parameter	EPR	EPS	IPS	PS
Bioactivity (Pa) Pa > Pi				
A	0.287	0.287	0.287	0.287
B	0.176	0.176	0.176	0.176
C	0.224	0.224	0.224	0.224
Bioactivity (*P*) Pa > Pi				
A	0.249	0.249	0.249	0.249
B	0.073	0.073	0.073	0.073
C	0.098	0.098	0.098	0.098

Pa: Activity probability; Pi: Probability of being inactive A: Antiviral (Picornavirus); B: Antioxidant; C: Anticarcinogenic.

The HIA data are calculated from bioavailability and absorption, being a crucial factor in predicting the viability of medication absorption through the small intestine [87]. Low-absorbed compounds have HIA of 0–20%, moderately absorbed 20–70%, and highly absorbed 70–100%. The values, in Table 7, refer to compounds that have a high human intestinal absorption.

While the prediction of toxicity is an indispensable factor in the screening of new drugs, the results are favourable as the tests ran on rats and mice were negative. The risk of heart disease (hER risk) is an important factor; and the molecules here analysed present a medium risk. The assessment of *in silico* toxicity in drug planning is an important factor, as it assists in determining the toxic dose in studies with animal models and decreases the number of guinea pigs infected by the disease [88].

In Table 8, PASS Online predicts both the probability of being active (Pa) and the probability of being inactive (Pi). Pa estimates the chance of the studied compound to belong to the subclass of active compounds and Pi estimates the chance of the compound to belong to the subclass of inactive compounds [69].

The compounds have potential activity against Picornavirus, which the best known of them is Rhinovirus, the one that causes the common cold in humans and is associated with severe respiratory infections [89]. They also have antioxidant effects, playing a crucial role in protecting healthy body cells against the oxidising action of free radicals [90]. And they are considered anticancer agents, through the negative tests ran on rats and mice.

Therefore, the ADMET *in silico* results for the EPR, EPS, IPS and PS molecules are promising for the continuity with the *in vitro* and *in vivo* tests with the SARS-CoV-2 strains. This is because they present activity against serious respiratory infections caused by Rhinovirus and absence of toxicity in the organisms of rats and mice.

4. Conclusion

Based on the results presented in this study, the imidazole alkaloids epiisopiloturine, epiisopilosine, isopilosine and pilosine have shown indications as possible inhibitors of the main SARS-CoV-2 protease. This is a fact observed through the high thermodynamic stability, chemical reactivity based on quantum descriptors (especially epiisopilosine, isopilosine and pilosine), the strong interactions with the main amino acid residues in the active site of the enzyme M^{pro}, the constant interaction activity during the 50 ns of simulation, the favourable pharmacokinetic profile and the absence of toxicity for rats and mice.

However, only the epiisopilosine and epiisopiloturine molecules were investigated in a dynamic manner, what is promising regarding the energy stability and the affinity of interaction with the target. In this way, the *in silico* data is relevant and allows the continuation of the steps *in vitro* and *in vivo* in the search for a treatment or cure for COVID-19.

Acknowledgements

We are grateful for the institutional support of CENAPAD-UFC, IFPI, IFPA, IFMA, UFPI and UESPI. In particular to the Research Laboratory of the Computational Quantum Chemistry and Drug Planning Group (GQQC&PF/UESPI). F.C.A.L. suggested the idea of doing a computational investigation. E.R.A.S., R.M.R. and R.K.M.C. performed computational work. A.N.C., E.R.A.S. and R.M.R. analysed and interpreted the data. J.L.S., E.R.A.S. and R.M.R. wrote the manuscript. F.C.A.L. guided the entire development of the study. All authors reviewed and approved the manuscript.

Disclosure statement

No potential conflict of interest was reported by the author(s).

References

[1] Huynh T, Wang H, Luan B. In silico exploration of the molecular mechanism of clinically oriented drugs for possibly inhibiting SARS-CoV-2's main protease. J Phys Chem Lett. 2020;11:4413–4420. doi:10.1021/acs.jpclett.0c00994

[2] Zhu N, Zhang D, Wang W, et al. A novel coronavirus from patients with pneumonia in China, 2019. New Engl J Med. 2020;382:727–733. doi:10.1056/NEJMoa2001017

[3] Lancet T. Global coalition to accelerate COVID-19 clinical research in resource-limited settings. J Lancet Healthy Longevity. 2020;395:1322–1325. doi:10.1016/S0140-6736(20)30798-4.

[4] OPAS/OMS Brazil. (2020). Fact sheet - COVID-19 (disease caused by the new coronavirus). Brasilia, DF, Brazil. https://www.paho.org/bra/ (accessed 30.11.2020).

[5] Zhang L, Lin D, Sun X, et al. Crystal structure of SARS-CoV-2 main protease provides a basis for design of improved a-ketoamide inhibitors. Science. 2020;368:409–412. doi:10.1126/science.abb3405

[6] Anand K, Palm GJ, Mesters JR, et al. Structure of coronavirus main proteinase reveals combination of a chymotrypsin fold with an extra α-helical domain. EMBO J. 2002;21:3213–3224. doi:10.1093/emboj/cdf327

[7] Yang H, Yang M, Ding Y, et al. The crystal structures of severe acute respiratory syndrome vírus main protease and its complex with an inhibitor. Proc Nat Acad Sci. 2003;100:13190–13195.doi:10.1073/pnas.1835675100

[8] Jin Z, Du X, Xu Y, et al. Structure of M^{pro} from SARS-CoV-2 and discovery of its inhibitors. Nature. 2020;582:289–293. doi:10.1038/s41586-020-2223-y

[9] Yang H, Xie W, Xue X, et al. Design of wide-spectrum inhibitors targeting coronavirus main proteases. PLoS Biol. 2005;3:e324. doi:10.1371/journal.pbio.0030324

[10] Wang F, Chen C, Tan W, et al. Structure of main protease from human coronavirus NL63: insights for amplo espectro anti-coronavirus drug design. Sci Rep. 2016;6:22677. doi:10.1038/srep22677

[11] Aanouz I, Belhassan A, El-Khatabi K, et al. Moroccan medicinal plants as inhibitors against SARS-CoV-2 main protease: computational investigations. J Biomol Struct Dyn. 2020. doi:10.1080/07391102.2020.1758790.

[12] Ferreira ET, Santos ES, Monteiro JS, et al. The use of medicinal and phytotherapy plants: An integrational review on the nurses performance. Braz J Health Rev. 2019;2:1511–1523. https://www.brazilianjournals.com/index.php/BJHR/article/view/1383 (accessed 20.04.2020).

[13] Lima DF, Lima LI, Rocha JA, et al. Seasonal change in main alkaloids of jaborandi (Pilocarpus microphyllus Stapf ex Wardleworth), an economically important species from the Brazilian flora. PLoS ONE. 2017;12:e0170281. doi:10.1371/journal.pone.0170281.

[14] Duke JA. Handbook of medicinal herbs. 2nd ed New York: CRC Press; 2002; 896 p.

[15] Devi R, Singh V, Chaudhary AK. Antidiabetic activity of pilocarpus microphyllus extract on streptozotocin-induced diabetic mice. Int J Pharm Sci Rev Res. 2010;5:87–92. https://www.semanticscholar.org/paper/ANTIDIABETIC-ACTIVITY-OF-PILOCARPUS-MICROPHYLLUS-ON-Devi-Singh/9f0c6d63d0de9a46337316684b215293a7e8de7c#citing-papers (accessed 25.04.2020).

[16] Agban Y, Lian J, Prabakar S, et al. Nanoparticle cross-linked collagen shields for sustained delivery of pilocarpine hydrochloride. Int J Pharm. 2016;501:96–101. doi:10.1016/j.ijpharm.2016.01.069

[17] Gil-Montoya JA, Silvestre FJ, Barrios R, et al. Treatment of xerostomia and hyposalivation in the elderly: a systematic review. Oral Medicine Oral Pathology and Oral Surgery. 2016;21:e355–e366. doi:10.4317/medoral.20969.

[18] Guimarães MA, Campelo YD, Véras LM, et al. Nanopharmaceutical approach of epiisopiloturine alkaloid carried in liposome system: preparation and in vitro schistosomicidal activity. J Nanosci Nanotechnol. 2014;14:4519–4528. doi:10.1166/jnn.2014.8248

[19] Guimarães MA, de Oliveira RN, Véras LMC, et al. Anthelmintic activity in vivo of epiisopiloturine against juvenile and adult worms of *Schistosoma mansoni*. PLoS Negl Trop Dis. 2015;9:e0003656. doi:10.1371/journal.pntd.0003656

[20] Rocha JA, Rego NCS, Carvalho BTS, et al. Computational quantum chemistry, molecular docking, and ADMET predictions of imidazole alkaloids of Pilocarpus microphyllus with schistosomicidal properties. PLoS ONE. 2018;13:e0198476. doi:10.1371/journal.pone.0198476.

[21] Silva VG, Silva RO, Damasceno SRB, et al. Anti-inflammatory and antinociceptive activity of epiisopiloturine, an imidazole alkaloid isolated from Pilocarpus microphyllus. J Nat Prod. 2013;76:1071–1077. doi:10.1021/np400099m

[22] Nicolau LAD, Carvalho NS, Pacífico DM, et al. Epiisopiloturine hydrochloride, an imidazole alkaloid isolated from *Pilocarpus microphyllus* leaves, protects against naproxen-induced gastrointestinal damage in rats. Biomed Pharmacother. 2017;87:188–195. doi:10.1016/j.biopha.2016.12.101

[23] Rocha JA, Andrade IM, Véras LMC, et al. Anthelmintic, antibacterial and cytotoxicity activity of imidazole alkaloids from Pilocarpus microphyllus leaves. Phytother Res. 2017;31:624–630. doi:10.1002/ptr.5771

[24] Lima Neto JX. (2019). Estudo em complexos fármaco-receptor utilizando bioquímica quântica [Quantum biochemistry study in drug-receptor complexes]. 140f. Thesis (Doctorate in Biochemistry). Federal University of Rio Grande do Norte, Natal, Brazil. Portuguese. https://repositorio.ufrn.br/jspui/handle/123456789/26645 (accessed 02.05.2020).

[25] Das S, Sarmah S, Lyndem S, et al. An investigation into the identification of potential inhibitors of SARS-CoV-2 main protease using molecular docking study. J Biomol Struct Dyn. 2020; doi:10.1080/07391102.2020.1763201.

[26] Kadan, R. U., Roy, N. Recent Trends in drug likeness prediction: a comprehensive review of In silico methods. Indian J Pharm Sci. 2007;69: 609–615. doi:10.4103/0250-474X.38464

[27] Berman HM, Westbrook J, Feng Z, et al. The protein data Bank. Nucleic Acids Res. 2000;28:235–242. doi:10.1093/nar/28.1.235

[28] Santos AP, Moreno PRH. Pilocarpus spp.: a survey of its chemical constituents and biological activities. Braz J Pharm Sci. 2004;40:115–137. doi:10.1590/S1516-93322004000200002.

[29] Abreu IN, Mazzafera P, Eberlin MN, et al. Characterization of the variation in the imidazole alkaloid profile of Pilocarpus microphyllus in different seasons and parts of the plant by electrospray ionization mass spectrometry fingerprinting and identification of novel alkaloids by tandem mass spectrometry. Rapid Commun Mass Spectrom. 2007;21:1205–1213. doi:10.1002/rcm.2942

[30] Véras LMC, Cunha VRR, Lima FCDA, et al. Industrial scale Isolation, structural and spectroscopic characterization of epiisopiloturine from pilocarpus microphyllus Stapf leaves: a promising alkaloid against schistosomiasis. PLoS ONE. 2013;8:e66702. doi:10.1371/journal.pone.0066702

[31] Dennington R, Keith TA, Millam JM. (2016). GaussView, version 6, Semichem Inc., Shawnee Mission, KS. https://gaussian.com/gaussview6/ (accessed 03.05.2020).

[32] Costa RA, Junior ESA, Lopes GBP, et al. Structural, vibrational, UV–vis, quantum-chemical properties, molecular docking and anti-cancer activity study of annomontine and N-hydroxyannomontine β-carboline alkaloids: a combined experimental and DFT approach. J Mol Struct. 2018;1171:682–695. doi:10.1016/j.molstruc.2018.06.054

[33] Costa RA, Oliveira KMT, Nunomura RCS, et al. Quantum chemical properties investigation and molecular docking analysis with DNA topoisomerase II of β-carboline indole alkaloids from Simaba guianensis: a combined experimental and theoretical DFT study. Struct Chem. 2018;29:299–314. doi:10.1007/s11224-017-1029-5

[34] Frisch MJ, Trucks GW, Schlegel HB, et al. Gaussian09, Revision C.01. Wallingford (CT): Gaussian, Inc.; 2010; https://gaussian.com (accessed 05.05.2020).

[35] Lee C, Yang W, Parr RG. Development of the colle-salvetti correlation-energy formula into a functional of the electron-density. Phys Rev B. 1988;37:785–789. doi:10.1103/PhysRevB.37.785

[36] Becke AD. Density-functional thermochemistry. III. The role of exact exchange. J Chem Phys. 1993;98:5648–5652. doi:10.1063/1.464913

[37] Mclean AD, Chandler GS. Contracted Gaussian-basis sets for molecular calculations. 1. second row atoms, Z = 11–18. J Chem Phys. 1980;72:5639–5648. doi:10.1063/1.438980

[38] Krishnan R, Binkey JS, Seeger R, et al. Self-consistent molecular orbital methods. XX. Basis set for correlated wave-functions. J Chem Phys. 1980;72:650–654. doi:10.1063/1.438955

[39] Janak JF. Proof that in density-functional Theory. Phys Rev B. 1978;18:7165–7168. doi:10.1103/PhysRevB.18.7165

[40] Perdew JP, Parr RG, Levy M, et al. Density-functional theory for fractional particle number: derivative discontinuities of the energy. Phys Rev Lett. 1982;49:1691–1694. doi:10.1103/PhysRevLett.49.1691

[41] Parr RG, Chattaraj PK. Principle of maximum hardness. J Am Chem Soc. 1991;113:1854–1855. doi:10.1021/ja00005a072

[42] Parr RG, Szentpály LV, Liu S. Electrophilicity index. J Am Chem Soc. 1999;121:1922–1924. doi:10.1021/ja983494x

[43] Pettersen EF, Goddard TD, Huang CC, et al. UCSF Chimera–a visualization system for exploratory research and analysis. J Comput Chem. 2004;25:1605–1612. doi:10.1002/jcc.20084

[44] Goodsell DS, Morris G, Olson AJ. Automated docking of flexible ligands: applications of AutoDock. J Mol Recogn. 1996;9:1–5. doi:10.1002/(SICI)1099-1352(199601)9:1<1::AID-JMR241>3.0.CO;2-6

[45] Huey R, Morris GM, Forli S. (2012). Using AutoDock4 and AutoDock Vina with AutoDockTools: A tutorial. The Scripps Research Institute. https://www.yumpu.com/en/document/view/52169976/using-autodock-4-and-autodock-vina-with-autodocktools-a-tutorial (accessed 08.05.2020).

[46] Trott O, Olson AJ. Autodock Vina: improving the speed and accuracy of docking with a new scoring function, efficient optimization, and multithreading. J Comput Chem. 2010;31:455–461. doi:10.1002/jcc.21334.

[47] Ravindranath PA, Forli S, Goodsell DS, et al. AutoDockFR: advances in protein-ligand docking with explicitly specified binding site flexibility. PLoS Comput Biol. 2015;11:e1004586. doi:10.1371/journal.pcbi.1004586

[48] Morris GM, Goodsell DS, Halliday RS, et al. Automated docking using a Lamarckian genetic algorithm and an empirical binding free energy function. J Comput Chem. 1998;19:1639–1662. doi:10.1002/(SICI)1096-987X(19981115)19:14<1639::AID-JCC10>3.0.CO;2-B

[49] Barros RO, Junior FLCC, Pereira JWS, et al. Interaction of drugs candidates with various SARS-CoV-2 receptors: an in silico study to combat COVID-19. J Proteome Res. 2020; doi:10.1021/acs.jproteome.0c00327.

[50] Biovia DS. (2020). Discovery studio visualizer, San Diego: Dassault Systèmes. https://3dsbiovia.com/products/collaborative-science/biovia-discovery-studio/visualization.html (accessed 15.05.2020).

[51] Breneman CM, Wiberg KB. Determining atom-centered monopoles from molecular electrostatic potentials. The need for high sampling density in formamide conformational analysis. J Comput Chem. 1990;11:361–373. doi:10.1002/jcc.540110311

[52] Chirlian LE, Francl MM. Atomic charges derived from electrostatic potentials: a detailed study. J Comput Chem. 1987;8:894–905. doi:10.1002/jcc.540080616

[53] Mei Y, Simmonett AC, Pickard FC, et al. Numerical study on the partitioning of the molecular polarizability into fluctuating charge and induced atomic dipole contributions. J Phys Chem A. 2015;119:5865–5882. doi:10.1021/acs.jpca.5b03159

[54] Gordon JC, Myers JB, Folta T, et al. Hþþ: a server for estimating pKas and adding missing hydrogens to macromolecules. Nucleic Acids Res. 2005;33:w368–w371. doi:10.1093/nar/gki464

[55] Abraham MJ, Van Der Spoel D, Lindahl E, et al. (2018). The GROMACS development team. GROMACS user manual version 2018.1. www.gromacs.org (accessed 20.05.2020).

[56] Oostenbrink C, Villa A, Mark AE, et al. A biomolecular force field based on the free enthalpy of hydration and solvation: the GROMOS force-field parameter sets 53A5 and 53A6. J Comput Chem. 2004;25:1656–1676. doi:10.1002/jcc.20090

[57] Arcanjo DDR, Vasconcelos AG, Nascimento LA, et al. Structure-function studies of BPP-BrachyNH 2 and synthetic analogues thereof with Angiotensin I-converting enzyme. Eur J Med Chem. 2017;139:401–411. doi:10.1016/j.ejmech.2017.08.019

[58] Van der Spoel D, Van Maaren PJ, Berendsen HJC. A systematic study of water models for molecular simulation: derivation of water models optimized for use with a reaction field. J Chem Phys. 1998;108:10220–10230. doi:10.1063/1.476482

[59] Ramos RM, Perez JM, Baptista LA, et al. Interaction of wild type, G68R and L125M isoforms of the arylamineN-acetyltransferase from mycobacterium tuberculosis with isoniazid: a computational study on a new possible mechanism of resistance. J Mol Model. 2012;18:4013–4024. doi:10.1007/s00894-012-1383-6

[60] Nosé S, Klein ML. Constant pressure molecular dynamics for molecular systems. Mol Phys. 1983;50:1055–1076. doi:10.1080/00268978300102851

[61] Parrinello M, Rahman A. Polymorphic transitions in single crystals: a new molecular dynamics method. J Appl Phys. 1981;52:7182–7190. doi:10.1063/1.328693

[62] Hess B, Bekker H, Berendsen HJC, et al. LINCS: a linear constraint solver for molecular simulations. J Comput Chem. 1997;18:1463–1472. doi:10.1002/(SICI)1096-987X(199709)18:12<1463::AID-JCC4>3.0.CO;2-H.

[63] Darden T, York D, Pedersen L. Particle mesh Ewald: an N, log(N) method for Ewald sums in large systems. J Appl Phys. 1993;98:10089–10092. doi:10.1063/1.464397.

[64] Lemkul J. From proteins to perturbed hamiltonians: a suite of tutorials for the GROMACS-2018 molecular simulation package [Article v1.0]. Living J Comput Mol Sci. 2019;1:1–53. doi:10.33011/livecoms.1.1.5068

[65] Verli H. Bioinformática da biologia à flexibilidade molecular [Bioinformatics from biology to molecular flexibility]. 1st ed São Paulo: SBBq; 2014; 282 p. Portuguese. https://www.ufrgs.br/bioinfo/ebook/ (accessed 23.12.2020).

[66] Lagorce D, Bouslama L, Becot J, et al. FAF-Drugs4: free ADME-tox filtering computations for chemical biology and early stages drug discovery. Bioinformatics. 2017;33:3658–3660. doi:10.1093/bioinformatics/btx491

[67] Lee SK, Chang GS, Lee IH, et al. The PreADME: pc-based program for batch prediction of adme properties. EuroQSAR. 2004;9:5–10. https://scholar.google.com/scholar?cluster=9485303528805910143&hl=pt-BR&as_sdt=2005&sciodt=0,5 (accessed 10.06.2020).

[68] Daiana A, Michielin O, Zoete V. SwissADME: a free web tool to evaluate pharmacokinetics, drug-likeness and medicinal chemistry friendliness of small molecules. Sci Rep. 2017;7:1–13. doi:10.1038/srep42717

[69] Filimonov DA, Lagunin AA, Gloriozova TA, et al. Prediction of the biological activity spectra of organic compounds using the PASS online web resource. Chem Heterocycl Compd (NY). 2014;50:444–457. doi:10.1007/s10593-014-1496-1

[70] Kramer C, Ting A, Zheng H, et al. Learning medicinal chemistry absorption, distribution, metabolism, excretion, and toxicity (ADMET) rules from cross-company matched molecular Pairs analysis (MMPA). J Med Chem. 2018;61:3277–3292. doi:10.1021/acs.jmedchem.7b00935

[71] Sá ERA, Nascimento LA, Lima FCA. Termodinâmica: Uma Proposta de Ensino a partir da Química Computacional [Thermodynamics: a teaching proposal based on computational chemistry]. Virtual J Chem. 2020;12:795–808. Portuguese. doi:10.21577/1984-6835.20200062.

[72] Honório KM, da Silva ABF. An AM1 study on the electron-donating and electron-accepting character of biomolecules. Int J Quantum Chem. 2003;95:126–132. doi:10.1002/qua.10661

[73] Da Silva RR, Ramalho TC, Santos JM, et al. On the limits of highest-occupied molecular orbital driven reactions: the frontier effective-for-reaction molecular orbital concept. J Phys Chem. 2006;110:1031–1040. doi:10.1021/jp054434y

[74] Maltarollo VG, Silva DC, Honório KM. Advanced QSAR studies on PPARδ ligands related to metabolic diseases. J Braz Chem Soc. 2012;23:85–95. doi:10.1590/S0103-50532012000100013

[75] Pang X, Zhou L, Zhang M, et al. Two rules on the protein-ligand interaction. Open Conf Proc J. 2012;3:70–80. doi:10.2174/2210289201203010070

[76] Costa AN, Sá ERA, Bezerra RDS, et al. Constituents of buriti oil (Mauritia flexuosa L.) like inhibitors of the SARS-coronavirus main peptidase: an investigation by docking and molecular dynamics. J Biomol Struct Dyn. 2020. doi:10.1080/07391102.2020.1778538.

[77] Arnott JA, Planey SL. The influence of lipophilicity in drug discovery and design. Expert Opin Drug Discov. 2012;7:863–875. doi:10.1517/17460441.2012.714363

[78] Storpirtis S, Gai MN, Campos DR, et al. Farmacocinética básica e aplicada [Basic and applied pharmacokinetics]. Rio de Janeiro: Guanabara Koogan; 2011; 240 p. Portuguese.

[79] Gurunga AB, Bhattacharjeea A, Ali MA. Exploring the physicochemical profile and the binding patterns of selected novel anticancer himalayan plant derived active compounds with macromolecular targets. Inf Med Unlocked. 2016;5:1–14. doi:10.1016/j.imu.2016.09.004

[80] Ertl P, Rohde B, Selzer P. Fast calculation of molecular polar surface area as a sum of fragment-based contributions and its application to the prediction of drug Transport properties. J Med Chem. 2000;43:3714–3717. doi:10.1021/jm000942e

[81] Lipinski CA, Lombardo F, Dominy BW, et al. Experimental and computational approaches to estimate solubility and permeability in drug discovery and development settings. Adv Drug Deliv Rev. 2001;46:3–26. doi:10.1016/S0169-409X(00)00129-0

[82] Lagorce D, Douguet D, Miteva MA, et al. Computational analysis of calculated physicochemical and ADMET properties of protein-protein interaction inhibitors. Sci Rep. 2017;7:46277. doi:10.1038/srep46277

[83] Bickerton GR, Paolini GV, Besnard J, et al. Quantifying the chemical beauty of drugs. Nat Chem. 2012;4:90–98. doi:10.1038/nchem.1243

[84] Brown RD, Hassan M, Waldman M. Combinatorial library design for diversity, cost efficiency, and drug-like character. J Mol Graphics Model. 2000;18:427–437. doi:10.1016/S1093-3263(00)00072-3

[85] Kobayashi M, Sada N, Sugawara M, et al. Development of a new system for prediction of drug absorption that takes into account drug dissolution and pH change in the gastro-intestinal tract. Int J Pharm. 2001;221:87–94. doi:10.1016/S0378-5173(01)00663-9

[86] Irvine JD, Takahashi L, Lockhart K, et al. MDCK (Madin-Darby Canine Kidney) cells: a tool for membrane permeability screening. J Pharm Sci. 1999;88:28–33. doi:10.1021/js9803205

[87] Souza J, Freitas ZMF, Storpirtis S. In vitro models for the determination of drug absorption and a prediction of dissolution/absorption relationships. Braz J Pharm Sci. 2007;43:515–527. doi:10.1590/S1516-93322007000400004.

[88] Sripriya N, Ranjith Kumar M, Ashwin Karthick N, et al. In silico evaluation of multispecies toxicity of natural compounds. Drug Chem Toxicol. 2019;21:1–7. doi:10.1080/01480545.2019.1614023.

[89] Costa LF. (2012). Rinovírus humano em infecções respiratórias agudas em crianças menores de cinco anos de idade: fatores envolvidos no agravamento da doença [Human rhinovirus in acute respiratory infections in children under five years of age: factors involved in the worsening of the disease]. 71f. Thesis (Doctorate in Biological Sciences) - Federal University of Uberlândia, Uberlândia, Brazil. Portuguese. https://repositorio.ufu.br/handle/123456789/16573 (accessed 08.08.2020).

[90] Kuskoski EM, Asuero AG, Troncoso AM, et al. Application of several chemical methods to determine antioxidant activity in fruit pulp. Food Sci Tech. 2005;25:726–732. doi:10.1590/S0101-20612005000400016.